International Journal of Thermal Sciences 48 (2009) 2092–2099

Contents lists available at ScienceDirect

International Journal of Thermal Sciences

journal homepage: www.elsevier.com/locate/ijts

Numerical investigation into thermal mixing efficiency in Y-shaped channel using Lattice Boltzmann method and field synergy principle

Cheng-Chi Chang, Yue-Tzu Yang, Tzu-Hsiang Yen, Cha'o-Kuang Chen*

Department of Mechanical Engineering, National Cheng Kung University, Tainan, Taiwan 70101, ROC

ARTICLE INFO

Article history:
Received 26 June 2008
Received in revised form
3 March 2009
Accepted 3 March 2009

Keywords:
Lattice Boltzmann method
Field synergy principle
Thermal mixing flow

ABSTRACT

This study employs the lattice Boltzmann method to simulate the thermal mixing efficiency of two-dimensional, incompressible, steady-state low Reynolds number flows in a Y-shaped channel. The effects of introducing a staggered arrangement of wave-like and circular obstacles into the mixing section of the Y-shaped channel are systematically examined. The simulation results demonstrate that both types of obstacle yield an effective improvement in the thermal mixing efficiency compared to that achieved in a Y-channel with a straight mixing section. Adopting the field synergy principle, it is demonstrated that the enhanced mixing efficiency is the result of an increased intersection angle between the velocity vector and the temperature gradient within the channel.

1. Introduction

The lattice Boltzmann method (LBM) has emerged as a powerful computational technique for simulating fluid flows and modeling the physics of fluids [1]. In conventional computational fluid dynamics (CFD) simulations, macroscopic variables such as the mass and velocity are derived by solving the continuity and Navier–Stokes equations. However, the LBM approach is based on microscopic models and mesoscopic kinetic equations and involves modeling the flow system by tracking the evolution of individual particle distributions using a discretized single-particle phase space distribution function similar to that described by the traditional Boltzmann BGK equation. The fundamental concept of the LBM technique is to construct simplified kinetic models which reflect the essential physics of the microscopic or mesoscopic processes in such a way that the averaged properties at the macroscopic scale are consistent with those obtained using the corresponding macroscopic equations. Researchers have demonstrated the successful application of the LBM approach to the solution of a wide variety of real-world scientific and engineering problems [2–4].

Adopting the simplified thermal model presented by Peng et al. [5] and the D2Q9 LBM model, Chen et al. [6–8] simulated incompressible, steady-state low Reynolds number flows in a channel with a backward-facing step. The results obtained for the velocity and temperature fields were found to be in good agreement with the published experimental and numerical data. One of the principal advantages of the LBM scheme is its straightforward treatment of non-rectangular boundary conditions. Filippova and Hanel [9] applied an enhanced bounce-back rule to extend the LBM method to the modeling of fluid flows in channels with curved walls. Mei et al. [10] improved the numerical stability of the solution procedure by introducing a revised expression for $\Delta < (1/2)$ (Δ: the fraction of the intersected link in the fluid region). Guo et al. [11] extended the extrapolation scheme proposed by Chen et al. [12] to develop a new treatment for curved boundaries with second-order accuracy.

Guo et al. [13] and Wang et al. [14] studied the mechanisms involved in convective heat transfer and proposed a novel approach for enhancing these mechanisms in fluid systems with parabolic-type flow structures. In their approach, the convection term was transformed into a dot product of the velocity vector and the temperature gradient and it was shown that the convective heat transfer effect could be enhanced by raising the value of the integral of the convective term over the thermal boundary layer. The objective of the proposed approach was to improve the uniformity of the velocity and temperature profiles and to reduce the intersection angle between the dimensionless velocity vector and the temperature gradient. Guo et al. [13] referred to this approach as the field synergy (coordination) principle. Tao et al. [15,16] extended the field synergy concept from parabolic to elliptic fluid flow systems and to other transport phenomena. Guo et al. [17] introduced the concept of a field synergy number to

* Corresponding author. Tel.: +886 6 2757575x62140; fax: +886 6 2342081.
E-mail address: ckchen@mail.ncku.edu.tw (Cha'o-K. Chen).

1290-0729/$ – see front matter © 2009 Elsevier Masson SAS. All rights reserved.
doi:10.1016/j.ijthermalsci.2009.03.001

Nomenclature

c	lattice streaming speed
c_s	speed of sound
g_α	energy distribution function
g_α^{eq}	equilibrium distribution function for g_α
H	channel height
d	obstacle diameter
w	inter-obstacle spacing
Pr	Prandtl number
p	pressure
Re	Reynolds number
T	temperature
U	maximum velocity in inlet
$\vec{V}$	velocity vector
f_α	density distribution function
f_α^{eq}	equilibrium distribution function for f_α

Greek symbols

τ_v	relaxation time for f_α
τ_c	relaxation time for g_α
ε	internal energy
χ	diffusivity
ρ	density
υ	kinematic viscosity
δx	lattice spacing
δt	time step
θ	intersection angle between velocity vector and temperature gradient

Subscripts

m	mean
w	wall
h	high
l	low

quantify the degree of synergy between the velocity and temperature fields at both the entire flow system and the heat transfer domain.

Using the curved boundary treatment scheme presented by Guo et al. [11], the current study simulates the velocity and temperature fields within two-dimensional, incompressible, steady-state low Reynolds number flows in a Y-shaped channel. The simulations focus specifically on the thermal mixing efficiency obtained in Y-channels containing either a straight mixing section or a mixing section with a staggered arrangement of wave-like or circular obstacles. Applying the field synergy principle, it is shown that the obstacles improve the thermal mixing efficiency by increasing the intersection angle between the velocity vector and the temperature gradient within the mixing section.

2. Simulation methodology

2.1. Lattice Boltzmann method

The present simulations use the 2-dimensional, 9-speed (D2Q9) LBM model with a single-time Bhatnagar–Gross–Krook (BGK) relaxation collision operator. In the D2Q9 model, the lattice streaming speed is given by $c = \delta x/\delta t = \delta y/\delta t$, where δx and δy are the grid spacings in the x- and y-directions, respectively, and correspond to the distances moved by each particle in the x- and y-directions during each time step of the LBM simulation. The discrete velocities in the D2Q9 model are defined as follows:

$$\begin{aligned}&\vec{e}_\alpha = (0,0), \quad \alpha = 0, \textit{rest particle}\\ &\vec{e}_\alpha = (\cos\theta_\alpha, \sin\theta_\alpha)c, \ \theta_\alpha = (\alpha-1)\pi/2, \quad \alpha = 1,2,3,4\\ &\vec{e}_\alpha = \sqrt{2}(\cos\theta_\alpha, \sin\theta_\alpha)c, \ \theta_\alpha = (\alpha-5)\pi/2+\pi/4, \quad \alpha = 5,6,7,8.\end{aligned} \tag{1}$$

The evolution equations for the density distribution function and the energy distribution function are given respectively by

$$f_\alpha(\vec{x}+\vec{e}_\alpha\delta t, t+\delta t) - f_\alpha(\vec{x},t) = -\frac{1}{\tau_v}\left[f_\alpha(\vec{x},t) - f_\alpha^{eq}(\vec{x},t)\right], \tag{2}$$

$$g_\alpha(\vec{x}+\vec{e}_\alpha\delta t, t+\delta t) - g_\alpha(\vec{x},t) = -\frac{1}{\tau_c}\left[g_\alpha(\vec{x},t) - g_\alpha^{eq}(\vec{x},t)\right], \tag{3}$$

where τ_v is the viscosity-based dimensionless relaxation time and τ_c is the dimensionless relaxation time for energy transport. The local equilibrium density distribution has the form

$$f_\alpha^{eq} = w_\alpha\rho\left[1 + \frac{3\,\vec{e}_\alpha\cdot\vec{V}}{c^2} + \frac{9}{2}\frac{(\vec{e}_\alpha\cdot\vec{V})^2}{c^4} - \frac{3}{2}\frac{\vec{V}^2}{c^2}\right], \tag{4}$$

$$w_0 = \frac{4}{9}, \quad w_\alpha = \frac{1}{9} \ \textit{for} \ \alpha = 1,2,3,4, \quad w_\alpha = \frac{1}{36} \ \textit{for} \ \alpha = 5,6,7,8.$$

After evolving the density distribution function and energy distribution function at the discrete lattices, the density and velocity are determined respectively from

$$\rho = \sum_\alpha f_\alpha, \quad \rho\vec{V} = \sum_\alpha \vec{e}_\alpha f_\alpha. \tag{5}$$

The equilibrium energy distribution functions, g, can be written as

$$g_0^{eq} = -\frac{2\rho\varepsilon}{3}\frac{\vec{V}^2}{c^2}, \tag{6}$$

$$g_{1,2,3,4}^{eq} = \frac{\rho\varepsilon}{9}\left[\frac{3}{2} + \frac{3}{2}\frac{\vec{e}_\alpha\cdot\vec{V}}{c^2} + \frac{9}{2}\frac{(\vec{e}_\alpha\cdot\vec{V})^2}{c^4} - \frac{3}{2}\frac{\vec{V}^2}{c^2}\right], \tag{7}$$

$$g_{5,6,7,8}^{eq} = \frac{\rho\varepsilon}{36}\left[3 + 6\frac{\vec{e}_\alpha\cdot\vec{V}}{c^2} + \frac{9}{2}\frac{(\vec{e}_\alpha\cdot\vec{V})^2}{c^4} - \frac{3}{2}\frac{\vec{V}^2}{c^2}\right], \tag{8}$$

where $\varepsilon = RT$, in which R is the gas constant and T is the temperature. The macroscopic temperature can then be calculated as

$$\rho\varepsilon = \sum_\alpha g_\alpha. \tag{9}$$

The Navier–Stokes equation and continuity equation are then given by

$$\partial_t\rho + \nabla\cdot(\rho\vec{V}) = 0, \tag{10}$$

$$\partial_t(\rho\vec{V}) + \nabla\cdot(\rho\vec{V}\vec{V}) = -\nabla p + \upsilon\left[\nabla^2(\rho\vec{V}) + \nabla(\nabla\cdot(\rho\vec{V}))\right], \tag{11}$$

where $p = c_s^2\rho$ is the pressure, and is derived from the equation of state for an ideal gas, $c_s = c/\sqrt{3}$ is the speed of sound, and υ is the kinematic viscosity, and is given by

$$\upsilon = \frac{(2\tau_v - 1)}{6}\frac{(\delta x)^2}{\delta t}. \tag{12}$$

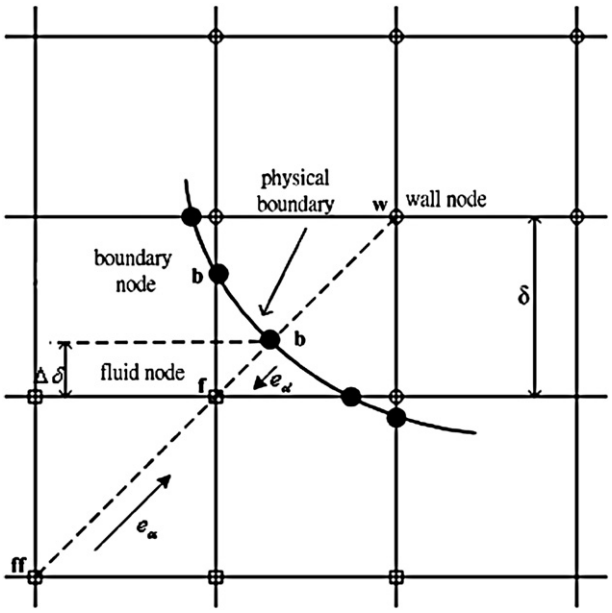

Fig. 1. Schematic illustration showing curved boundary and lattice nodes.

In general, the Mach number of a flow is defined as $M = \vec{V}/c_s$. A low Mach number assumption can be applied as the nearly incompressible limit is approached, i.e. $M \ll 1$. Under these conditions, the incompressible continuity equation and the Navier–Stokes equation are expressed respectively as

$$\nabla \cdot \vec{V} = 0, \tag{13}$$

$$\partial_t \vec{V} + \vec{V} \cdot \nabla \vec{V} = -\frac{\nabla p}{\rho} + \upsilon \nabla^2 \vec{V}. \tag{14}$$

The Chapman–Enskog expansion of the thermal energy distribution function can be used to recover the macroscopic energy equation, i.e.

$$\partial_t(\rho\varepsilon) + \nabla \cdot (\rho \vec{V} \varepsilon) = \chi \nabla^2(\rho\varepsilon). \tag{15}$$

Furthermore, the diffusivity, χ, is determined by

$$\chi = \frac{2}{3}\left(\tau_c - \frac{1}{2}\right)\delta t. \tag{16}$$

In the current simulations, the density distribution function and energy distribution function given in Eqs. (2) and (3), respectively, are both solved using a two-step procedure, i.e. a collision step followed by a streaming step. The streaming step requires little computational effort since it simply advances the data from the neighboring lattice points, while the collision step is completely localized.

2.2. Non-rectangular boundary treatment

This study applies the curved boundary treatment proposed by Guo et al. [11] to model the wave-like and circular obstacles introduced in the mixing section of the Y-shaped channel. This boundary treatment decomposes the distribution function, f_α, at a wall node into equilibrium and non-equilibrium parts. The non-equilibrium part of the function is approximated by that of the neighboring fluid node along the link, while the equilibrium part is determined from an imaginary equilibrium distribution in which the boundary condition is enforced. As shown in Fig. 1, the link between the fluid node, $\vec{x}_f$, and the wall node, $\vec{x}_w$, intersects the physical boundary at $\vec{x}_b$. The fraction of the intersected link within the fluid region is given by

$$\Delta = \left(\left|\vec{x}_f - \vec{x}_b\right|\right) / \left(\left|\vec{x}_f - \vec{x}_w\right|\right). \tag{17}$$

As described above, $f_\alpha(\vec{x}_w, t)$ is decomposed into $f_\alpha^{eq}(\vec{x}_w, t)$ and $f_\alpha^{ne}(\vec{x}_w, t)$, respectively. The equilibrium part of $f_\alpha(\vec{x}_w, t)$, i.e. $f_\alpha^{eq}(\vec{x}_w, t)$, can be defined approximately as

$$f_\alpha^{eq}(\vec{x}_w, t) = w_\alpha \rho_w \left[1 + \frac{3\vec{e}_\alpha \cdot \vec{V}_w}{c^2} + \frac{9}{2}\frac{(\vec{e}_\alpha \cdot \vec{V}_w)^2}{c^4} - \frac{3}{2}\frac{\vec{V}_w^2}{c^2}\right], \tag{18}$$

where $\vec{V}_w$ is an approximation of $\vec{V}_w = \vec{V}(\vec{x}_w)$ and $\rho_w \equiv \rho(\vec{x}_f)$ is an approximation of $\rho_w = \rho(\vec{x}_w)$. It is reasonable to determine $\vec{V}_w$ via a process of linear extrapolation using either $\vec{V}_{w1} = (\vec{V}_b + (\Delta - 1)\vec{V}_f)/\Delta$ or $\vec{V}_{w2} = (2\vec{V}_b + (\Delta - 1)\vec{V}_{ff})/(1 + \Delta)$ and $\vec{V}_w = \vec{V}_{w1} = (\vec{V}_b + (\Delta - 1)\vec{V}_f)/\Delta$ for $\Delta \geq 0.75$ and $\vec{V}_w = \Delta \vec{V}_{w1} + (1 - \Delta)\vec{V}_{w2}$ for $\Delta < 0.75$. Meanwhile, Guo et al. [11] defined the non-equilibrium part of $f_\alpha(\vec{x}_w, t)$ as $f_\alpha^{ne}(\vec{x}_w, t) = f_\alpha^{ne}(\vec{x}_f, t)$ for $\Delta \geq 0.75$ and $f_\alpha^{ne}(\vec{x}_w, t) = \Delta f_\alpha^{ne}(\vec{x}_f, t) + (1 - \Delta) f_\alpha^{ne}(\vec{x}_{ff}, t)$ for $\Delta < 0.75$. The post-collision distribution function, $f_\alpha^+(\vec{x}_w, t)$, can then be obtained as

$$f_\alpha^+(\vec{x}_w, t) = f_\alpha^{eq}(\vec{x}_w, t) + (1 - 1/\tau_v) f_\alpha^{ne}(\vec{x}_w, t). \tag{19}$$

The temperature at node $\vec{x}_f$ can be approximated by interpolating the temperature at the neighboring points based on the fraction of the intersected link within the fluid region.

2.3. Simulation conducted

In conducting the present simulations, it is necessary to construct suitable conditions for f_α and g_α based on the macroscopic flow variables. The wave-like and circular obstacles are assumed to be thermally isolated. As a result, they interrupt the fluid flow in the Y-channel, but play no direct role in the heat transfer process. As shown in Fig. 2, the fluid streams introduced though the upper ($\overline{ab}$) and lower ($\overline{cd}$) inlets are brought into contact

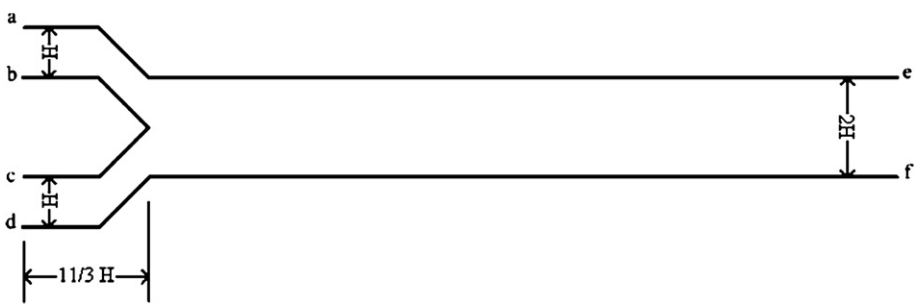

Fig. 2. Geometric configuration of Y-shaped channel with straight mixing section.

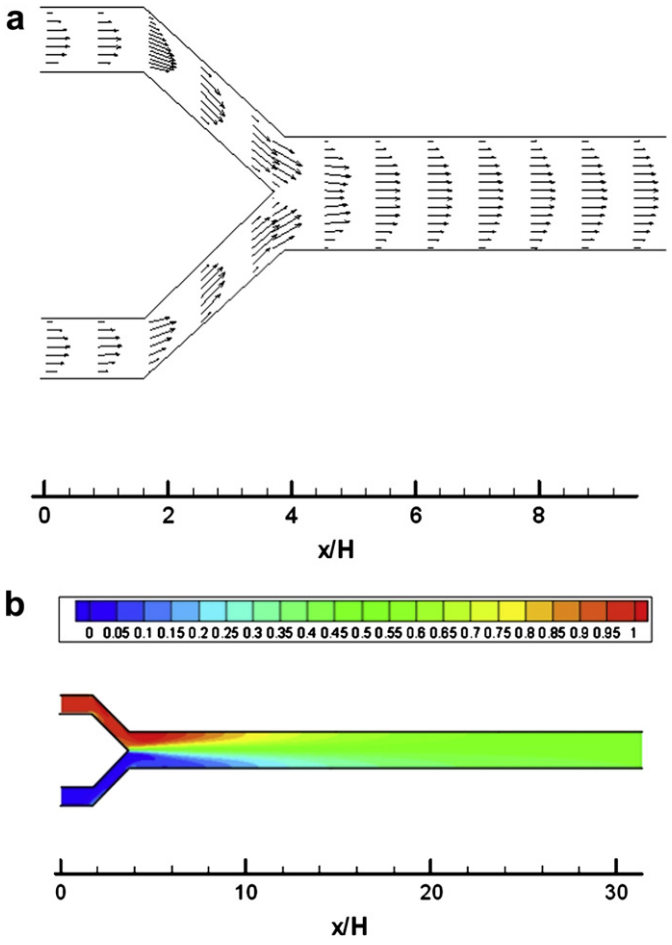

Fig. 3. (a) Velocity field and (b) temperature distribution in Y-shaped channel with straight mixing section (Re = 105, Pr = 0.7).

at an angle of 45° in the entrance region of the mixing section. The heights of the two inlet channels and the main mixing channel are denoted by H and $2H$, respectively. The simulations are performed using a uniform grid (901*181) and terminate in accordance with the following convergence criteria:

$$\frac{\sum_{i,j}\left\|\vec{V}(x_{i,j},t+\delta t)-\vec{V}(x_{i,j},t)\right\|}{\sum_{i,j}\left\|\vec{V}(x_{i,j},t)\right\|}\le 1.0\times 10^{-6}, \tag{20}$$

$$\frac{\sum_{i,j}\left\|T(x_{i,j},t+\delta t)-T(x_{i,j},t)\right\|}{\sum_{i,j}\left\|T(x_{i,j},t)\right\|}\le 1.0\times 10^{-6}, \tag{21}$$

where $\|*\|$ is the L_2 norm.

In specifying the boundary conditions, a constant velocity flow of 0.05 is applied at both inlets. This velocity is specifically chosen to be less than 10% of the speed of sound in order to prevent the formation of significant compressibility effects. The Reynolds number of the flow is defined as $\mathrm{Re} = U_{\max}\times 2H/\upsilon$. Using the bounce-back rule incorporated in the non-equilibrium distribution function proposed by Zou and He [18], the equilibrium density distribution function is derived from the pressure and velocity conditions imposed at the first lattice column in the computational domain. At the channel outlet, a fixed pressure boundary condition is imposed in terms of the equilibrium distribution function and the velocity components of the flow are extrapolated from those in the upstream direction. The bounce-back rule [18] is applied to establish a no-slip boundary condition at the wall surface. The density distribution function at the boundary must satisfy the following condition:

$$f_\alpha^{neq}=f_\beta^{neq}, \tag{22}$$

where e_α and e_β have opposite directions.

In modeling the temperature distribution within the channel, the thermal energy distribution function at the boundary satisfies

$$g_\alpha^{neq}-e_\alpha^2 f_\alpha^{neq}=-\left(g_\beta^{neq}-e_\beta^2 f_\beta^{neq}\right). \tag{23}$$

The temperature of the wall is used when calculating g^{eq} for the boundary nodes in order to satisfy the given temperature. In the current simulations, the temperature at the wall is assigned in accordance with a Neumann boundary condition. In the general Dirichlet type condition, the given temperature is applied directly at the boundary. However, in the current study, the temperature at the boundary is obtained by converting the Neumann type condition to the Dirichlet condition using the conventional second-order finite difference approximation method [19]. For a given temperature gradient, the temperature at the boundary can be calculated by

$$\left.\frac{\partial T}{\partial y}\right|_{x,1}=\frac{-3T_{x,1}+4T_{x,2}-T_{x,3}}{2\Delta y}. \tag{24}$$

Equation (24) yields the Dirichlet type boundary condition for both adiabatic and constant heat flux boundary conditions.

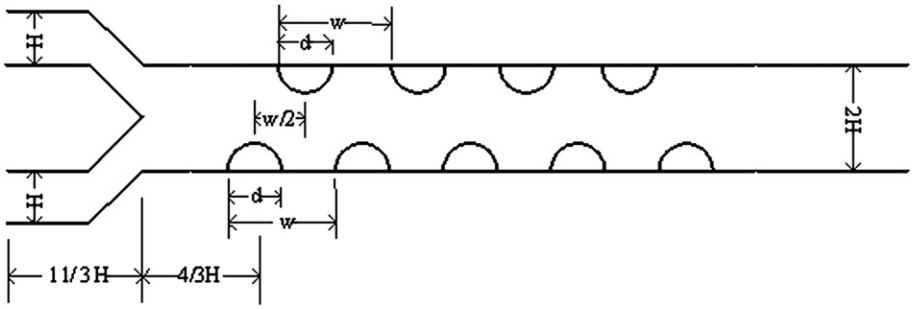

Fig. 4. Geometric configuration of Y-shaped channel with wave-like obstacles in mixing section.

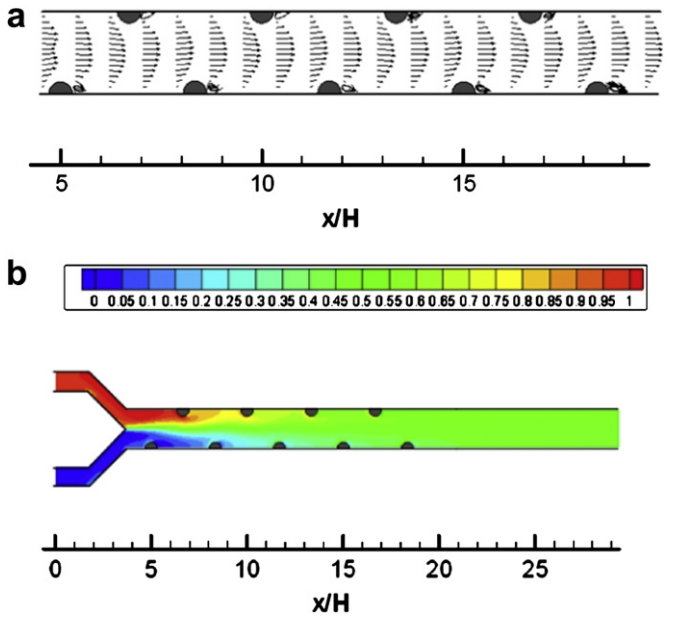

Fig. 5. (a) Velocity field and (b) temperature distribution in Y-shaped channel with wave-like obstacles in mixing section (Re = 105, Pr = 0.7, $d/H = 0.6$, $w/H = 10/3$).

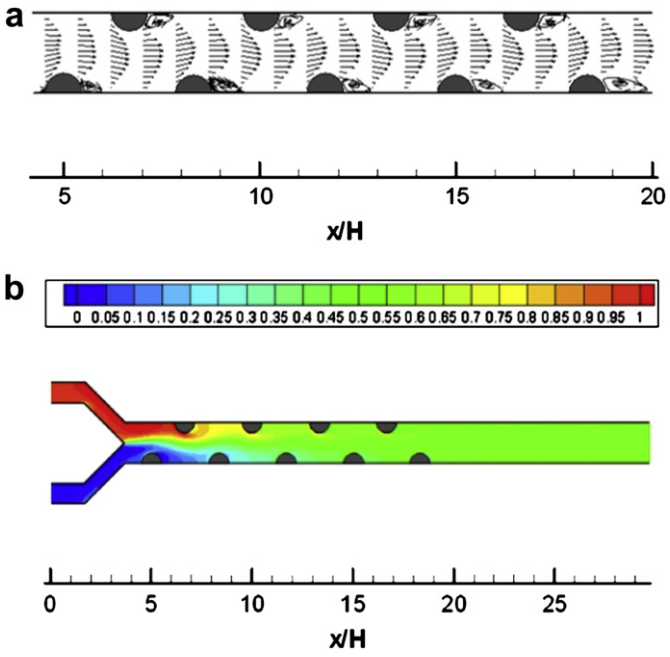

Fig. 6. (a) Velocity field and (b) temperature distribution in Y-shaped channel with wave-like obstacles in mixing section (Re = 105, Pr = 0.7, $d/H = 0.9$, $w/H = 10/3$).

3. Field synergy principle

In this study, the field synergy principle is applied to interpret the simulation results. According to Guo et al. [13] and Wang et al. [14], convection heat transfer such as that which takes place within the current Y-shaped channel can be regarded as a combined heat conduction and fluid motion mechanism. Equation (25), derived from [13,14], provides a general insight into convective heat transfer. This equation suggests that heat transfer in the current Y-shaped channel can be enhanced in one of three different ways, namely increasing the Reynolds and Prandtl numbers, increasing the fullness of the dimensionless velocity and temperature profiles, or reducing the intersection angle between the dimensionless velocity vector and the temperature gradient.

$$Re\ Pr \int (\vec{V} \cdot \nabla T) \mathrm{d}y = Nu, \tag{25}$$

where

$$\vec{V} \cdot \nabla T = |\vec{V}||\nabla T| \cos\theta, \tag{26}$$

$$\theta_m = \frac{\sum A_i \theta_i}{\sum A_i}, \tag{27}$$

where θ is the intersection angle, θ_m is the average intersection angle between the velocity vector and the temperature gradient in the computation domain, A_i is the area of the small control volume and θ_i is the intersection angle of each grid. Note that in accordance with [15], if the local value of θ is greater than 90°, its value is taken as $(180^\circ - \theta)$ when added to the summation of the intersection angle in Eq. (27).

4. Results and discussion

We have tested the calculation results effected by particle number and the particle number of the present paper is adoptable.

Within calculation domain, we set the outlet pressure equal to 0.9 times the inlet pressure and nonslip boundary condition is adopted. The inlet temperatures are T_h and T_l and the rear channel is long enough so that the outlet temperature is fully developed. The thermal boundary conditions on the wall are adiabatic.

4.1. Case I – Y-shaped channel with straight mixing section

Fig. 3(a) illustrates the velocity vectors within the Y-shaped channel with a straight mixing section for the case of a Reynolds number of Re = 105 and a Prandtl number of 0.7. As shown, the parabolic velocity profiles of the two fluid streams entering the inlet channels are gradually distorted as they flow along the inclined channels toward the intersection region. However,

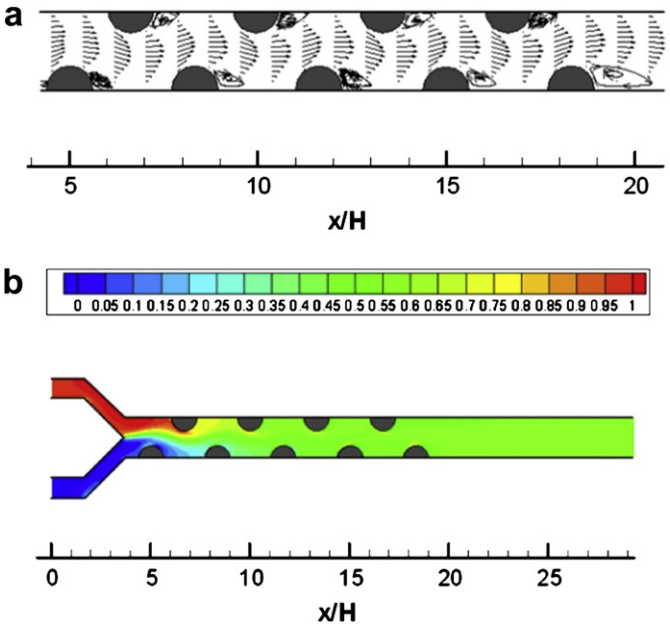

Fig. 7. (a) Velocity field and (b) temperature distribution in Y-shaped channel with wave-like obstacles in mixing section (Re = 105, Pr = 0.7, $d/H = 1.2$, $w/H = 10/3$).

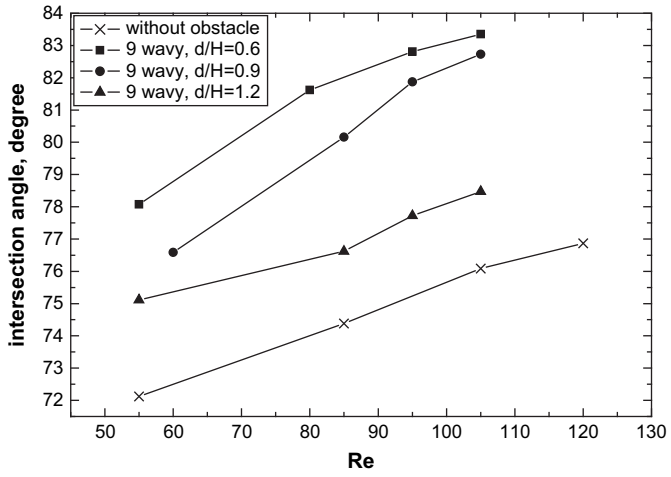

Fig. 8. Variation of average intersection angle with Reynolds number in mixing section with and without wave-like obstacles, respectively.

following an initial mixing of the two fluid streams, the parabolic velocity profile is gradually restored as the fluids flow along the mixing section and a fully developed condition is achieved. Fig. 3(b) presents the corresponding temperature distribution within the Y-shaped channel under the assumption that a fluid with a high temperature (T_h) is introduced through the upper inlet and a fluid with a low temperature (T_l) is introduced through the lower inlet. As shown, the colored contours represent the non-dimensional temperature, i.e. $T^* = (T - T_l)/(T_h - T_l)$, in increments of 0.05. It can be seen that a thermal mixing effect is initiated between the two fluid streams in the entrance region of the mixing section. The fluids are mixed continuously as they flow along the channel and it is found that a thermal equilibrium condition is attained at $x/H = 29$. The results presented in Fig. 3(b) correspond to a Reynolds number of $Re = 105$. Repeating the simulation using Reynolds numbers of $Re = 55$ and $Re = 85$, respectively, it is found that the corresponding thermal equilibrium conditions are attained at $x/H = 18$ and $x/H = 22$, respectively. These results are to be expected since fluid flows with a higher Reynolds number are characterized by a greater inertial force, and hence their thermal energy is dissipated more slowly. As a result, a greater mixing distance is required to achieve a stable thermal condition within the mixed fluid stream. The diffusion area of high and low temperature is wide and it needs longer channel to mix heat thoroughly.

4.2. Case II – Y-shaped channel with wave-like obstacles in mixing section

Fig. 4 presents the geometric configuration of the Y-shaped channel with nine wave-like obstacles within the mixing section, i.e. five obstacles along the lower wall and four along the upper wall. Each obstacle is in the form of a half-circle of diameter d. Neighboring obstacles on the same wall are arranged with a pitch w, and the obstacles on the upper wall are offset from those on the lower wall by a distance $w/2$. Fig. 5(a) illustrates the velocity field within the Y-shaped channel for the case of $Re = 105$, $Pr = 0.7$, $d/H = 0.6$ and $w/H = 10/3$. It can be seen that the obstacles squeeze the fluid stream as it passes between them resulting in a slight variation of the fluid velocity in the y-direction. Furthermore, it is noted that small recirculation zones are formed immediately behind each obstacle as a result of a pressure drag effect. Fig. 5(b) presents the corresponding temperature distribution within the Y-shaped channel. From observation, it is determined that a thermal equilibrium condition is attained at $x/H = 19$, which represents a significant reduction in the mixing distance compared to that obtained in the straight channel with no obstacles ($x/H = 29$). In other words, it is apparent that the wave-like obstacles are instrumental in promoting the thermal mixing efficiency within the Y-shaped channel.

Fig. 6(a) illustrates the velocity field within the Y-channel when the Reynolds number and Prandtl number remain unchanged at $Re = 105$ and $Pr = 0.7$, respectively, but the diameter of the wave-like obstacles is increased to $d/H = 0.9$. Comparing Fig. 6(a) with Fig. 5(a), it is apparent that the larger obstacle diameter increases the fluid contraction effect and expands the area of the recirculation zones behind each obstacle. The corresponding temperature distribution is shown in Fig. 6(b) and indicates that the thermal equilibrium condition is attained at $x/H = 20$. As stated above, when the fluid strikes an obstacle, a velocity component is generated in the y-direction. Consequently, the high temperature fluid in the upper region of the mixing section is directed toward the low temperature zone in the lower region of the mixing channel, and vice versa. Although the thermal mixing effect in the entrance region of the mixing section is enhanced when the obstacles have a larger diameter, the nozzle type effect induced as the fluid flows between opposing pairs of obstacles is also increased, and thus the flow has a greater velocity component in the x-direction. As a result, the point of thermal equilibrium is displaced slightly along the mixing section compared to the case in which the obstacles have a smaller diameter.

Fig. 7(a) and (b) presents the velocity and temperature fields in the Y-shaped channel for the case where the obstacle diameter is further increased to $d/H = 1.2$. (Note that the values of Re, Pr and w/H are unchanged.). From inspection, it is determined that thermal equilibrium conditions are attained at $x/H = 22$. In this example, a rapid thermal mixing of the two fluid streams occurs in the entrance region of the mixing section due to the large flow disturbance caused by the obstacles. However, compared to the examples shown in Figs. 5(a) and 6(a), the larger diameter of the obstacles in Fig. 7(a) increases the x-direction velocity component in the central region of the stream and therefore delays the full

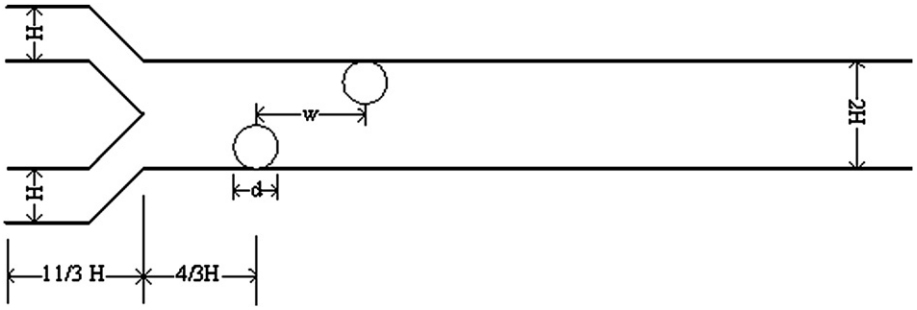

Fig. 9. Geometric configuration of Y-shaped channel with circular obstacles in mixing section.

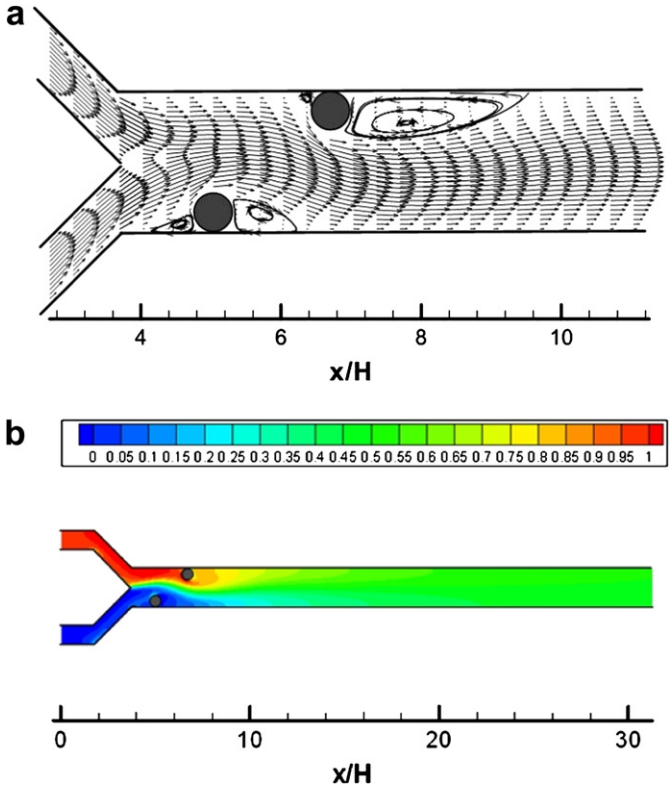

Fig. 10. (a) Velocity field and (b) temperature distribution in Y-shaped channel with circular obstacles (Case A).

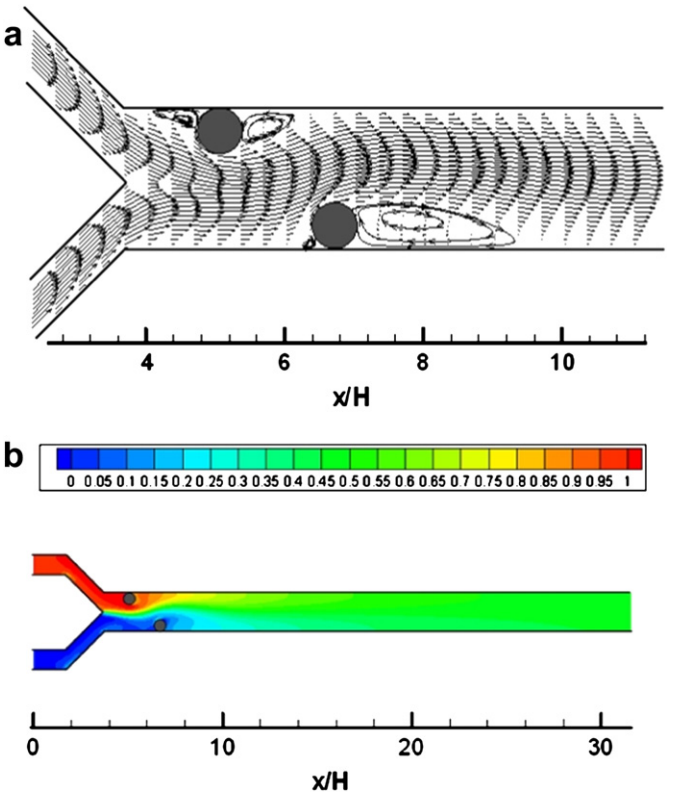

Fig. 11. (a) Velocity field and (b) temperature distribution in Y-shaped channel with circular obstacles (Case B).

mixing of the two streams. As a result, the point of thermal equilibrium is shifted in the downstream direction of the mixing section relative to that in the examples shown in Figs. 5(b) and 6(b) for obstacle diameters of $d/H = 0.6$ and 0.9, respectively.

Fig. 8 illustrates the average intersection angle between the velocity vector and the temperature gradient at various values of the Reynolds number in a Y-shaped channel with and without wave-like obstacles, respectively. For the purpose of heat transfer enhancement, the thermal of the system need to be transferred in or out the system. A better synergy means decreasing the intersection angle between velocity vector and temperature gradient. If the purpose is on thermal mixing problem, the thermal of the system need to be kept in the system. Then a better synergy means increasing the intersection angle. Applied the theory to the simulation results the understanding of thermal mixing effect will be more clear. From Fig. 8, it can be seen that the average intersection angle is always lower in the straight mixing section than in channels containing wave-like obstacles. As a result, introducing wave-like obstacles will inevitably improve the thermal mixing effect since a better synergy is obtained between the velocity field and the temperature field. Furthermore, decreasing the diameter of the wave-like obstacles increases the intersection angle between the velocity vector and the temperature field. As a result, the thermal mixing efficiency within the channel is improved as the obstacle diameter is reduced. Consequently, in the present simulations, the optimal thermal efficiency is obtained in the Y-channel containing wave-like obstacles with the smallest diameter, i.e. $d/H = 0.6$.

4.3. Case III – Y-shaped channel with circular obstacles within mixing section

Fig. 9 presents the geometric configuration of the Y-shaped channel with two circular obstacles within the mixing section. As shown, the obstacles have a diameter of d and are separated by a distance w. Fig. 10(a) illustrates the velocity field within the Y-shaped channel for the case of $Re = 105$, $Pr = 0.7$, $d/H = 0.6$ and $w/H = 5/3$. As shown, the obstacles are arranged such that the inlet streams initially encounter the obstacle on the lower wall. (Note that for convenience, this configuration is designated as Case A). It can be seen that the pressure drag effect induced as the flow passes between the two obstacles results in the formation of recirculation regions immediately upstream and downstream of both obstacles. Of these four recirculation structures, that behind the upper obstacle is particularly large. Fig. 10(b) presents the corresponding temperature distribution within the Y-shaped channel. From

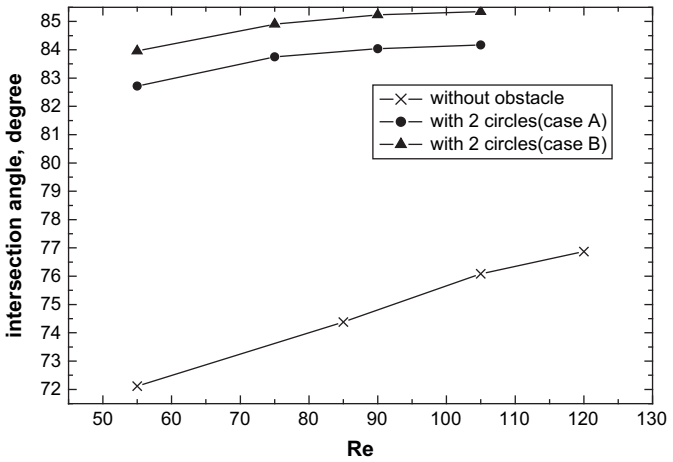

Fig. 12. Variation of average intersection angle with Reynolds number in mixing section with and without circular obstacles, respectively.

inspection, it is found that the point of thermal equilibrium is located at $x/H = 22$.

Fig. 11(a) presents the velocity field in the Y-shaped channel when the positions of the two circular obstacles are reversed such that the flow encounters the obstacle on the upper surface before that on the lower surface. (Note that for convenience, this configuration is designated as Case B). Comparing Fig. 11(a) with Fig. 10(a), it can be seen that the two velocity fields are symmetrical to one another, but are otherwise identical. However, a slight difference is found in the temperature fields in the two channels. As shown in Fig. 11(b), the inversion of the two obstacles causes the point of thermal equilibrium to move to $x/H = 18$ (compared to $x/H = 22$ in Fig. 10(b)). In general, heat transfer always takes place from a high temperature region to a low temperature region. Observing Figs. 10(a) and 11(a), it is apparent that the initial direction of the velocity field opposes the temperature gradient in Case A, but is aligned with the temperature gradient in Case B. As a result, the thermal mixing efficiency is enhanced in Fig. 11(b), and thus thermal equilibrium conditions are attained within a shorter mixing distance.

Fig. 12 illustrates the variation of the average intersection angle between the velocity vector and the temperature gradient with the Reynolds number in a Y-shaped channel with and without circular obstacles, respectively. The results indicate that the introduction of the obstacles increases the average intersection angle. Furthermore, it can be seen that Case B, in which the first obstacle encountered by the fluid is located on the upper wall of the mixing section, yields a greater intersection angle. Consequently, in accordance with the field synergy principle, it can be predicted that Case B will yield a more efficient mixing efficiency. This prediction is confirmed by Figs. 10(b) and 11(b), which show that thermal equilibrium conditions are obtained at $x/H = 22$ in the Case A configuration, but at $x/H = 18$ in the Case B configuration.

5. Conclusions

This study has simulated two-dimensional, steady-state low Reynolds number flows in a Y-shaped channel using a single-relaxation-time scheme based on the D2Q9 LBM model and a simplified thermal model. The simulations have focused specifically on the thermal mixing efficiency of two fluid streams of different initial temperatures within a straight mixing section and in a mixing section incorporating wave-like or circular obstacles respectively. The different sizes of obstacles have been mainly considered. The simulations results have been interpreted in accordance with the field synergy principle. It has been shown that the enhanced thermal mixing efficiency obtained by introducing obstacles into the mixing section is a result of a higher intersection angle between the velocity vector and the temperature gradient. The results have also shown that in the case where the mixing section incorporates obstacles, a lower obstacle diameter yields an improved mixing effect due to the greater synergy between the velocity field and the temperature field.

References

[1] S. Chen, G.D. Doolen, Lattice Boltzmann method for fluid flows, Annual Review of Fluid Mechanics 30 (1998) 329–364.
[2] X. He, S. Chen, G.D. Doolen, A novel thermal model for the Lattice Boltzmann method in incompressible limit, Journal of Computational Physics 146 (1998) 282–300.
[3] D.A. Wolf-Gladrow, Lattice Gas Cellular Automata and Lattice Boltzmann Models: An Introduction, Springer-Verlag, Berlin, 2000.
[4] S. Succi, The Lattice Boltzmann Method for Fluid Dynamics and Beyond, Oxford Univ. Press, Oxford, England, U.K., 2001.
[5] Y. Peng, C. Shu, Y.T. Chew, Simplified thermal lattice Boltzmann model for incompressible thermal flows, Physical Review E 68 (2003) 026701.
[6] C.K. Chen, T.S. Yen, Y.T. Yang, Lattice Boltzmann method simulation of backward-facing step on convective heat transfer with field synergy principle, International Journal of Heat and Mass Transfer 49 (2006) 1195–1204.
[7] C.K. Chen, T.S. Yen, Y.T. Yang, Lattice Boltzmann method simulation of backward-facing step with double plates aligned at angle to flow direction, ASME Journal of Heat Transfer 128 (2006) 1176–1184.
[8] C.K. Chen, T.S. Yen, Y.T. Yang, Lattice Boltzmann method simulation of a cylinder in the backward-facing step flow with the field synergy principle, International Journal of Thermal Science 45 (2006) 982–989.
[9] O. Filippova, D. Hanel, Grid refinement for lattice-BGK models, Journal of Computational Physics 147 (1998) 219–228.
[10] Renwei Mei, Li-Shi Luo, Wei Shyy, An accurate curved boundary treatment in the lattice Boltzmann method, Journal of Computational Physics 155 (1999) 307–330.
[11] Zhaoli Guo, Chuguang Zheng, Baochang Shi, An extrapolation method for boundary conditions in lattice Boltzmann method, Physics of Fluids 14 (2002) 2007–2010.
[12] S. Chen, D. Martinez, R. Mei, On boundary conditions in lattice Boltzmann methods, Physics of Fluids 8 (1996) 2527–2536.
[13] Z.Y. Guo, D.Y. Li, B.X. Wang, A novel concept for convective heat transfer enhancement, International Journal of Heat Mass Transfer 41 (5) (1998) 2221–2225.
[14] S. Wang, Z.X. Li, Z.Y. Guo, Novel concept and device of heat transfer augmentation, in: Proceeding of 11th IHTC 5, 1998, pp. 405–408.
[15] W.Q. Tao, Y.L. He, Q.W. Wang, Z.G. Qu, F.Q. Song, A unified analysis on enhancing single phase convective heat transfer with field synergy principle, International Journal of Heat Mass Transfer 45 (2002) 4871–4879.
[16] W.Q. Tao, Z.Y. Guo, B.X. Wang, Field synergy principle for enhancing convective heat transfer-its extension and numerical verifications, International Journal of Heat Mass Transfer 45 (2002) 3849–3856.
[17] Z.Y. Guo, W.Q. Tao, R.K. Shah, The field synergy (coordination) principle and its applications in enhancing single phase convective heat transfer, International Journal of Heat Mass Transfer 48 (2005) 1797–1807.
[18] Q. Zou, X. He, On pressure and velocity boundary conditions for the lattice Boltzmann BGK model, Physics of Fluids 9 (1997) 1591–1598.
[19] C. Shu, Y. Peng, Y.T. Chew, Simulation of natural convection in a square cavity by Taylor series expansion and least square-based Lattice Boltzmann method, International Journal of Modern Physics C 13 (2002) 1399–1414.